Tunable and enhanced Faraday rotation induced by the epsilon-near-zero response of a Weyl semimetal

Jipeng Wu,[1,2] Leyong Jiang,[3] Xiaoyu Dai,[1] and Yuanjiang Xiang[1,*]

[1]*School of Physics and Electronics, Hunan University, Changsha 410082, China*

[2]*College of Railway Transportation, Hunan University of Technology, Zhuzhou 412007, China*

[3]*School of Physics and Electronics, Hunan Normal University, Changsha 410081, China*

(Received 22 December 2021; accepted 11 April 2022; published 25 April 2022)

In this paper, we theoretically study the Faraday (FR) rotation effect excited by a transverse-magnetic (TM)-polarized wave passing through a bulk Weyl semimetal (WSM). Results show that the FR angle maintains a large value ($\sim -21^\circ$) with high transmission ($|t_{pp}| \sim 87\%$), which is caused by the close transmission coefficient of $|t_{ps}|$ $|t_{ps}|$ and $|t_{pp}|$. What is more important, the FR angle can be further enhanced at the epsilon-near-zero (ENZ) frequency, where a maximum FR rotation angle (absolute value) of 45° has been obtained due to the sharp decreases of $|t_{pp}|$. Remarkably, the ENZ frequency of the WSM can be regulated by varying the Fermi energy and tilt degree, resulting in the tunable and enhanced FR angle at the different ENZ frequencies. Particularly, it is demonstrated that the incident angle should be declined with the increase of WSM thickness for enhancing the FR angle at the ENZ frequency. We also examine the effect of Weyl node separation on the FR angle. Our studies provide a simple and effective method to enhance and control the FR effect with a WSM or other topological semimetals.

DOI: 10.1103/PhysRevA.105.043519

I. INTRODUCTION

Magneto-optical (MO) phenomena, such as Faraday (FR) and Kerr rotations, can be excited when light interacts with magnetic materials, and exhibit practical application prospects in optical communication systems [1]. FR rotation acts as one of the well-known MO effects, in which the polarization of light denotes gyration when the light passes through the magnetic material under applied magnetic field [2]. The FR effect plays a key role in several devices, such as optical switches [3], isolators [4], and sensors [5]. However, the footprint of such devices cannot be promptly decreased to the scale adapted to the current optical components and integrated optical circuitry because of the weak features of the FR effect in the optical domain. Therefore, it plays a key role in enhancing the FR effect for satisfying the needs of practical application. Recently, various methods have been proposed to enlarge the FR angle, such as enhanced optical fields [6–10], electromagnetically induced transparency [11], etc. Nevertheless, to the best of our knowledge, such methods usually require a high applied magnetic field, which may restrict its practical application.

A Weyl semimetal (WSM), as a spectacular topological quantum state with nonmass Weyl fermions as quasiparticles, appears only when the symmetry of time inversion or spatial inversion is broken [12–14]. Similar to the famous semimetal graphene, WSM exhibits a Dirac-like linear dispersion, and thus is known as "three-dimensional graphene." Thanks to its Dirac-like linear dispersion, WSM denotes many prominent optical characteristics, such as unique optical nonlinearity [15,16], and adjustable terahertz plasmon resonance [17]. Differently, compared with the two-dimensional Hamiltonian of graphene, WSM reveals the three-dimensional Hamiltonian, which brings many peculiar physical properties, such as chiral anomalies [18], unconventional quantum Hall effect [19], etc. Notably, the Weyl nodes in a WSM serve as a source or sink of the Berry curvature, acting as a magnetic field in the momentum space [20–23], resulting in the optical responses in WSMs needing to be characterized by means of the modified Maxwell's equations, called axion electrodynamics [24,25]. Simultaneously, the off-diagonal components of the permittivity tensor exist due to the equivalent magnetic field in momentum space, resulting in the Faraday and Kerr effects [26,27]. Recently, a variety of optical effects based on WSM have been widely studied, such as the tunable Goos-Hänchen shift [28], giant Kerr effect [29], anomalous Hall effects [30–33], etc. Previously, it was also reported that the FR angle is proportional to the separation between Weyl nodes for thin WSM films [27]. Notably, the thickness of the film can be reduced to maintain a large FR angle by appropriately increasing Weyl node separation. Meanwhile, high transmission can be obtained by reducing the thickness of the film. Therefore, the possible enhancement of the FR effect with high transmission in Weyl based systems without applied magnetic field exhibits important research value.

Epsilon-near-zero (ENZ) materials, on the other hand, as a novel class of materials, exhibiting zero or near-zero permittivity at one or multiple wavelengths, have aroused widespread concern in photonics [34–36]. ENZ materials display many extraordinary optical properties, including field enhancement [37], strong coupling phenomena [38], large nonlinear responses [39,40], etc. Notably, the ENZ response has been found in WSMs and was used to realize tunable

[*]xiangyuanjiang@126.com

perfect absorption [41]. Therefore, WSMs with ENZ response provide what we believe is a different research platform to study the FR effect without applied magnetic field.

In this paper, we theoretically study the FR effect excited by the transverse-magnetic (TM)-polarized wave passing through a bulk WSM with thickness of 200 nm. A 4×4 magneto-optical matrix (MOM) is set up to obtain the calculation of the FR angle by using Maxwell's equations and boundary conditions. Results show that the FR angle maintains a large value (∼ –21°) with high transmission ($|t_{pp}| \sim 87\%$), and can be further enhanced. Analyses indicate that the large FR angle is caused by the situation where the cross transmission coefficient $|t_{ps}|$ is close to the transmission coefficient $|t_{pp}|$. The further enhanced FR angle with its absolute value of 45° is induced by the situation that at ENZ frequency, the transmission coefficient $|t_{pp}|$ decreases sharply, resulting in the existence of the condition that the associated ellipticity is equal to 1. Remarkably, the ENZ frequency of the WSM can be regulated by varying the Fermi energy and tilt degree, resulting in the tunable enhanced FR effect at different ENZ frequencies. Additionally, it is demonstrated that at ENZ frequency, the incident angle should be reduced with the increase of thickness of the WSM to enhance the FR angle. Finally, we find that the enhancement of the FR angle rises with the increase of the Weyl node separation of the WSM when the frequency is far from the ENZ frequency. We firmly believe our study may find practical applications in magneto-optical devices.

II. THEORETICAL MODEL AND METHOD

Firstly, a permittivity tensor is introduced to recognize the optical properties of bulk WSM. Because the mode dispersion diagram of WSM exhibits dependence on the temperature, impurities, and disorder, the temperature is considered as zero, and the effects of impurities and disorder are ignored for clarity. Generally, by breaking time-reversal symmetry, a system composed of two Weyl cones emerges, known as the WSM. Through stacking the topological insulator and ferromagnet blocks into multiple thin films, the WSM appears [12]. Around the two Weyl nodes, the low energy physics is denoted by the Weyl Hamiltonian [12,41,42], a 2×2 matrix, marked as "$s = \pm$,"

$$H_s(\vec{p}) = v_F[\beta_s(p_z - sQ) + s\vec{\sigma}(\vec{p} - sQ\vec{e}_z)], \tag{1}$$

where v_F exhibits the Fermi velocity, $\vec{\sigma}$ displays the Pauli matrix, and $\vec{e}_z$ is the unit vector along the z direction. The separation between two Weyl points along the z direction in momentum space is shown by $2|Q|$, and the sign of Q depends on the sign of the magnetization, which is treated as positive in this paper [41]. The parameters $\beta_\pm$ denote the tilt of the Weyl cones that dominates the change between the type-I and type-II phases. For a type-I WSM, the parameters $\beta_\pm$ satisfy $|\beta_\pm| < 1$, while the parameters $\beta_\pm$ satisfy $|\beta_\pm| > 1$ for the type-II WSM. For centrosymmetric materials with broken time-reversal symmetry, the condition $\beta = \beta_+ = -\beta_-$ is met, in which the value of β is considered as positive. Eventually, a dielectric constant model can be introduced to describe the optical properties of WSM, and the corresponding expression is detailed in Appendix A.

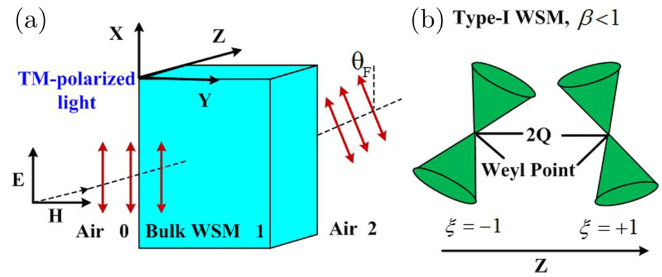

FIG. 1. Schematic exhibiting the FR angle excited by the TM-polarized wave passing through bulk WSM. (a) shows the TM-polarized wave passing through bulk WSM which is exposed in air, and the FR angle occurs. (b) exhibits a pair of tilted Weyl cones with opposite chirality in type-I WSM with a tilt degree $\beta < 1$, in which Q represents the Weyl node separation.

In order to study the FR rotation effect of light passing through the WSM, we theoretically design a simple structure, as shown in Fig. 1(a). A bulk WSM with thickness of d is exposed to air. Our structure is divided into three regions, air 0, WSM 1, and air 2. Considering a TM-polarized wave illuminating the bulk WSM with incident angle θ from air 0, transmission occurs at the contact surface of bulk WSM 1 and air 2, resulting in the existence of the FR effect. Figure 1(b) denotes the type-I ($\beta < 1$) WSMs, in which Q indicates the Weyl node separation along the z axis.

In our designed structure, for a pair of nodes separated along the z direction in the bulk Brillouin zone (BZ), the x-y plane has no Fermi arc states. The incident light illuminates the surface of bulk WSM (x-y plane), there is no surface conductivity at the $z = 0$ and d boundary since the projection of the vector is zero in this case; thus the tangential electric and magnetic fields stay continuous at the $z = 0$ and $z = d$ surface [27,43,44]. Therefore, the Fermi arc does not affect the transmission coefficient significantly. Due to the polarization separation of electromagnetic waves in the WSM [26,27], the traditional transfer matrix method is unsuitable for solving the transmission coefficients, and we introduce a 4×4 MOM to solve the problem. The solution procedure of the 4×4 magneto-optical matrix is detailed in Appendix B.

Ultimately, for a TM-polarized wave passing though the bulk WSM, the FR effect exists, and the relevant FR angle θ_F can be written as [45–47]

$$\tan(2\theta_F) = \frac{2\mathrm{Re}(\chi_F)}{1 - |\chi_F|^2}, \tag{2}$$

where the associated ellipticity $\chi_F = -t_{ps}/t_{pp}$.

III. DISCUSSIONS AND RESULTS

The feasibility of varying the Fermi energy serves as one of the salient characteristics of the WSM. Changing the Fermi energy about the charge neutrality point through doping, altering the temperature, or modifying the lattice constant of the material through pressure variations is successful [48–50]. To study the effect of Fermi energy on the ENZ response, we plot the real part of ε_{zz} as a function of frequency at different Fermi energies, as shown in Fig. 2(a). The relevant parameters are selected as $Q = 1\,\mathrm{nm}^{-1}$ and $\beta = 0.8$. It is found that there

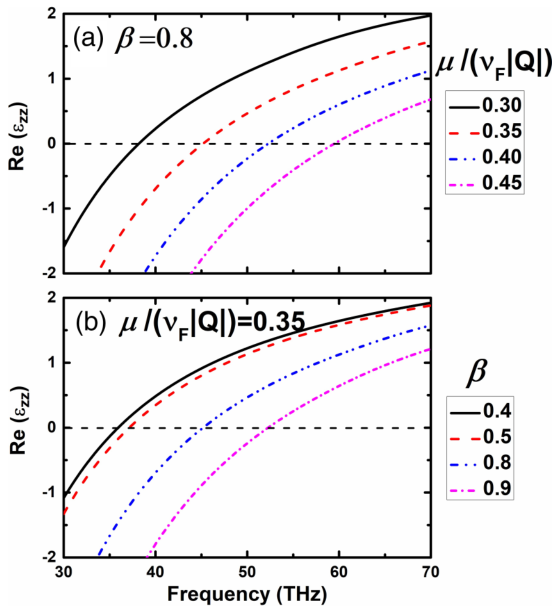

FIG. 2. The tunable ENZ response by varying the Fermi energy and tilt degree. (a) indicates the real part of ε_{zz} as a function of frequency at different Fermi energies. (b) exhibits the real part of ε_{zz} as a function of frequency at different tilt degrees.

always exist the ENZ response at different Fermi energies $0.3v_F|Q|$, $0.35v_F|Q|$, $0.4v_F|Q|$, and $0.45v_F|Q|$. With the increase of Fermi energy, the relative ENZ frequency increases. Specifically, the ENZ effect appears at 38.2 THz for Fermi energy of $0.3v_F|Q|$, at 45.2 THz for Fermi energy of $0.35v_F|Q|$, at 52.3 THz for Fermi energy of $0.4v_F|Q|$, and at 59.5 THz for Fermi energy of $0.45v_F|Q|$. Additionally, the tilt degree is another unique and extremely important parameter for determining the optical properties of the WSM. It is also known from the expression of ε_{zz} that the real part of ε_{zz} is directly affected by the tilt degree. Figure 2(b) exhibits the real part of ε_{zz} as a function of frequency at different tilt degrees. The relevant parameters are selected as $Q = 1\mathrm{nm}^{-1}$ and $\mu = 0.35v_F|Q|$. It is seen that the ENZ response always exists at different tilt degrees 0.4°, 0.5°, 0.8°, and 0.9°. As the tilt degree increases from 0.4° to 0.9°, the relative ENZ frequency rises from 35.95 to 52.28 THz. Therefore, the regulations of the ENZ response can be realized by simplify varying the Fermi energy and tilt degree, resulting in the feasible tunability of the FR effect.

Based on the calculated expression of the FR angle, it is obvious that it reaches its maximum absolute value of 45° when the value of $|\chi_F|$ is equal to 1. Unfortunately, for general magnetic materials, the FR angle is usually small and can be expressed as $\theta_F \approx \mathrm{Re}(\chi_F)$ for $|\chi_F| \ll 1$. To demonstrate the possibility of enhancement of the FR effect, Fig. 3(a) exhibits the FR angle as a function of frequency. The incident angle is optimized to 20°, and the thickness of the WSM is set as 200 nm. It is shown that the FR angle maintains a large value ($\sim$ –21°) when the frequency is far away from the ENZ frequency. Spectacularly, while the FR angle exhibits a large value, the transmission coefficient $|t_{pp}|$ also remains high ($\sim$87%), which denotes a significant difference from the general FR effect enhancement and is very useful in practical magneto-optical devices. Notably, when the frequency is near

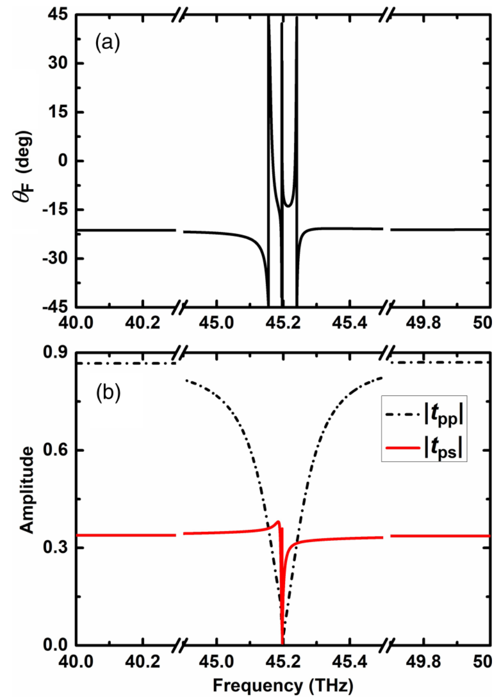

FIG. 3. The phenomenon of enhanced FR angle. (a) shows the FR angle as a function of frequency. (b) indicates the amplitude of $|t_{pp}|$ and $|t_{ps}|$ as a function of frequency, where the Fermi energy is set as $0.35v_F|Q|$, and the tilt degree is chosen as 0.8°. Other parameters are identical to those of Fig. 2.

the ENZ frequency, the FR effect can be further enhanced, and the FR angle obtains its maximum absolute value of 45° at three different frequencies. For explicating the causes of the above phenomena in detail, Fig. 3(b) shows the amplitude of $|t_{pp}|$ and $|t_{ps}|$ as a function of frequency. It is found that when the frequency is far away from the ENZ frequency, the amplitude of $|t_{ps}|$ is less than but close to $|t_{pp}|$, so a large FR effect exists, which is completely different from ordinary magnetic materials. Furthermore, due to the ENZ response of the WSM, the amplitude of $|t_{pp}|$ declines sharply and reaches its minimum value, nearly equal to 0 at ENZ frequency. Therefore, there exists the condition that the value of $|\chi_F|$ is equal to 1, resulting in the further enhancement of the FR effect. In Fig. 3(b), the situation that the value of $|\chi_F|$ is equal to 1 appears at three different frequencies, which is exactly consistent with the result of Fig. 3(a).

Notably, based on the above discussion, the FR effect can be further enhanced due to the ENZ response of the WSM. Meanwhile, the ENZ frequency can be regulated by changing the Fermi energy and tilt degree. Therefore, we can achieve the tunable enhanced FR effect at different frequencies by simply altering the Fermi energy and tilt degree. Figure 4 denotes the tunable enhanced FR angle at different frequencies by varying the Fermi energy and tilt degree. Figure 4(a) exhibits the FR angle as a function of frequency at different Fermi energies. It is seen that at different Fermi energies, the FR angle can be further enhanced at their corresponding ENZ frequencies. However, at frequencies far away from the ENZ frequency, the FR angle displays small differences at different Fermi energies. This is mainly caused by the fact

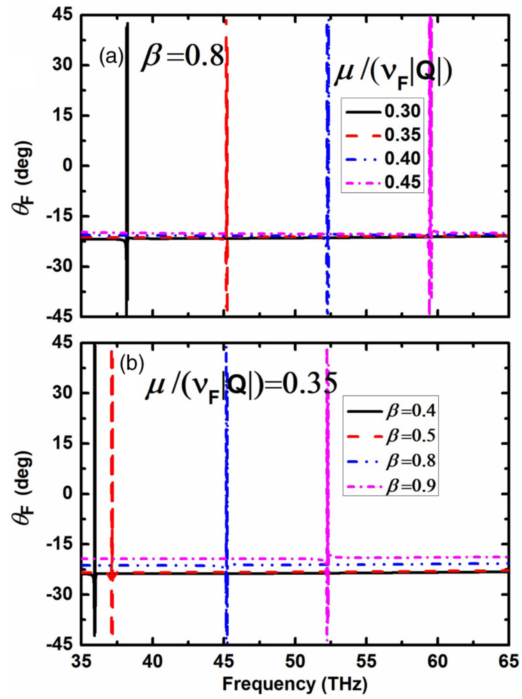

FIG. 4. The tunable enhanced FR angle by varying the Fermi energy and tilt degree. (a) shows the FR angle as a function of frequency at different Fermi energies. (b) exhibits the FR angle as a function of frequency at different tilt degrees. Other parameters are identical to those of Fig. 3.

that other dielectric constant components of the WSM also exhibit dependence on the Fermi energy, resulting in the small variation of transmission coefficients at different Fermi energies. Similarly, we can realize the enhancement of the FR angle at different frequencies by changing the tilt degree, as shown in Fig. 4(b). In other words, the tunability of the ENZ response by changing the Fermi energy and tilt degree enables the feasibility of the adjustable FR effect.

Notably, the transmission coefficients also display dependence on the incident angle and thickness of the WSM. Therefore, the variations of the incident angle and the thickness of the WSM will lead to the change of the FR angle. To further investigate the effect of incident angle and thickness of the WSM on the FR angle, Figure 5 exhibits the pseudocolor images of FR angle as functions of incident angle

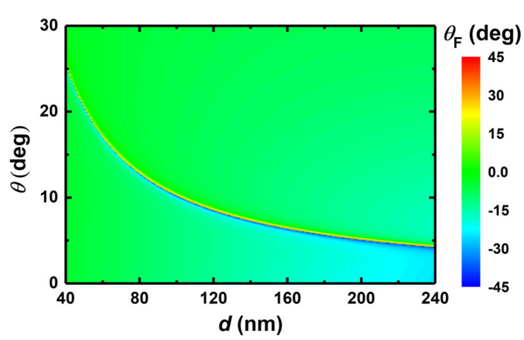

FIG. 5. Pseudocolor images of FR angle as functions of incident angle and thickness of WSM.

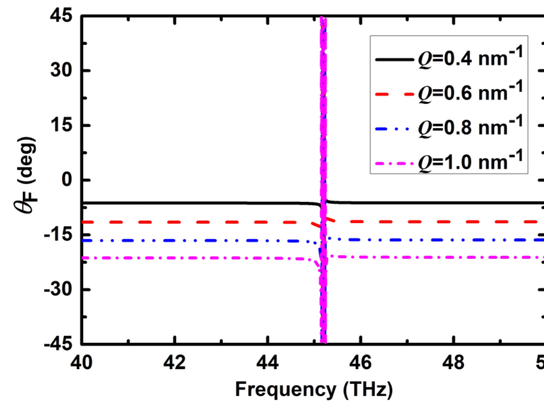

FIG. 6. The FR angle as a function of frequency at different Weyl node separations 0.4, 0.6, 0.8, and 1.0 nm^{-1}.

and thickness of WSM. The frequency of incident light is set at 45.2 THz, which corresponds to the ENZ frequency at tilt degree of 0.8°. Other relevant parameters are identical to those of Fig. 3. It is evident that the huge enhancement of the FR angle with its absolute value of 45° only appears in the angle range from 4° to 25°, and the FR angle stays basically constant at other incident angles. However, the huge enhancement of the FR angle with its absolute value of 45° can be maintained throughout our thickness range. Obviously, with the increase of thickness of the WSM, the incident angle should be reduced to enable the enhancement of the FR angle. Therefore, we should select a proper incident angle to enable the enhancement of the FR effect.

Finally, the Weyl nodes in the WSM act as a source or sink of the Berry curvature, acting as a magnetic field in the momentum space. The amplitude of the equivalent magnetic field can be described by the Weyl node separation. Generally, the off-diagonal components of the permittivity tensor emerge due to the existence of Weyl node separation, resulting in the Faraday and Kerr effects. To examine the effect of Weyl node separation on the FR angle, Figure 6 plots the FR angle as a function of frequency at different Weyl node separations 0.4, 0.6, 0.8, and 1.0 nm^{-1}, respectively. The energy cutoff, Fermi energy, and other relevant parameters are maintained identically to those in Fig. 3. Obviously, the huge enhancement of the FR angle with its absolute value of 45° can always be realized at these four different Weyl node separations based on the ENZ response. However, the FR angle displays differently at different Weyl node separations when the frequency is far away from the ENZ frequency. With the increase of Weyl node separation, the FR angle behaves as a larger enhancement. The main reason is that the cross transmission coefficient $|t_{ps}|$ increases with the increase of Weyl node separation, resulting in the amplitude of $|\chi_F|$ rising.

IV. CONCLUSIONS

In conclusion, we theoretically study the FR effect excited by the TM-polarized wave passing through a bulk WSM with a thickness of 200 nm. Due to the polarization separation of electromagnetic waves in WSM, the traditional transfer matrix method is unsuitable for solving the transmission coefficients, and we introduce a 4×4 MOM to solve the problem. It is found that the FR angle maintains a large value ($\sim -21^\circ$) with high transmission ($|t_{pp}| \sim 87\%$). Analyses indicate that the large FR angle is caused by the condition that the cross transmission coefficient $|t_{ps}|$ is less than but close to the transmission coefficient $|t_{pp}|$. The further enhanced FR angle with its absolute value of 45° can be obtained at the ENZ frequency. Remarkably, the ENZ frequency of the WSM can be regulated by simply varying the Fermi energy and tilt degree, resulting in the tunable enhanced FR angle at different frequencies. Finally, we find that the enhancement of the FR angle rises with the increase of the Weyl node separation of the WSM when the frequency is far from the ENZ frequency. Our studies provide a simple and effective method to enhance the FR effect.

ACKNOWLEDGMENTS

This research was supported by the Education Department of Hunan Province (Grants No. 20C0602 and No. 20C0603), the National Natural Science Foundation of China (Grants No. 61875133 and No. 11874269), the Natural Science Foundation of Hunan Province (Grants No. 2021JJ30135 and No. 2021JJ30149), and the Science and Technology Project of Shenzhen (Grants No. JCYJ20190808143801672, No. JCYJ20190808150803580, and No. JCYJ20180508152903208).

APPENDIX A: PERMITTIVITY OF TYPE-I WSMs

Generally, for a pair of nodes separated along the z direction in the bulk BZ, the permittivity tensor $\overline{\overline{\varepsilon}}$ of bulk WSM can be described as follows [41]:

$$\overline{\overline{\varepsilon}} = \begin{bmatrix} \varepsilon_{xx} & \varepsilon_{xy} & 0 \\ \varepsilon_{yx} & \varepsilon_{yy} & 0 \\ 0 & 0 & \varepsilon_{zz} \end{bmatrix}, \tag{A1}$$

where ε_{xx} and ε_{yy} denote the components of $\overline{\overline{\varepsilon}}$ parallel to the interfaces, and $\varepsilon_{xx} = \varepsilon_{yy} = \varepsilon_{||}$. The component ε_{zz} exhibits perpendicular to the interface. The off-diagonal components are described as $\varepsilon_{xy} = -\varepsilon_{yx} = i\gamma$, which can bring the polarization rotations, resulting in the existence of Faraday and Kerr effects [26,27]. All of the dielectric constant components mentioned above exhibit dependence on the frequency of incident light, in which the components $\varepsilon_{xx,yy}$ can be written analytically as [41]

$$\varepsilon_{xx,yy}(\omega) = 1 + \frac{\alpha}{3\pi}\left[\ln\left|\frac{4\Gamma^2}{4\mu^2-\omega^2}\right| - \frac{4\mu^2}{\omega^2} + i\pi\Theta(\omega - 2\mu)\right], \tag{A2}$$

where μ serves as the Fermi energy, $\alpha = e^2/(4\pi\varepsilon_0\hbar v_F)$ is the fine structure constant, the Fermi velocity $v_F = 10^6$ m/s, Γ denotes the energy cutoff which usually depends on the tilt parameter, and $\Theta(X)$ displays the usual step function. In the later discussions, the energy cutoff is chosen as high as $\Gamma = 8v_F|Q| \gg (\omega, \mu)$, so the effect of β on Γ can be ignored.

It is known from Eq. (A2) that $\varepsilon_{||}$ shows independence of the tilt parameter. For the case when the Weyl cones displays not tilted, $\beta = 0$, the diagonal components are equal, $\varepsilon_{zz} = \varepsilon_{||}$. Meanwhile, the off-diagonal component can be simplified to $\varepsilon_1 = -2v_F\alpha Q(\pi\omega)^{-1}$. Additionally, the value of the imaginary part of $\varepsilon_{||}$ exhibits positive when the frequency of the light wave satisfies $\omega > 2\mu$, while $\varepsilon_{||}$ denotes a real number in other cases.

Similarly, the dielectric constant component ε_{zz} is also a function of frequency, but also shows dependence on the tilt parameter. The expression of ε_{zz} displays very complex, and the numerical simulation method should be used to obtain its solutions. Fortunately, for type-I WSM, ε_{zz} can be approximately described as [41]

$$\varepsilon'_{zz} = 1 + \frac{\alpha\mu^2}{\pi\omega^2}\sum_{s=\pm}\frac{1}{\beta_s^3}\left\{\begin{array}{l} \frac{8}{3}\beta_s - 4\operatorname{arctanh}\beta_s + \ln\left|\frac{4\mu^2-\omega^2(1+\beta_s)^2}{4\mu^2-\omega^2(1-\beta_s)^2}\right| \\ +\frac{\omega^2}{12\mu^2}\sum_{t=\pm1}\left[\begin{array}{l} t(1+2t\beta_s)(1-t\beta_s)^2\ln\left|\frac{4\Gamma^2(1-t\beta_s)^2}{4\mu^2-\omega^2(1-t\beta_s)^2}\right| \\ -\frac{2\mu}{\omega}\left(\frac{4\mu^2}{\omega^2}+3-3\beta_s^2\right)\ln\left|\frac{2\mu-t\omega(1+t\beta_s)}{2\mu+t\omega(1+t\beta_s)}\right| \end{array}\right] \end{array}\right\}, \tag{A3}$$

$$\varepsilon''_{zz} = \frac{\alpha}{6}\sum_{s=\pm}\Theta\left(\omega - \frac{2\mu}{1+|\beta_s|}\right)\left(1 - \frac{1}{2}\left\{1 + \frac{3}{2|\beta_s|}\left(\frac{2\mu}{\omega}-1\right)\left[1 - \frac{1}{3\beta_s^2}\left(\frac{2\mu}{\omega}-1\right)^2\right]\right\}\Theta\left(\frac{2\mu}{1-|\beta_s|}-\omega\right)\right), \tag{A4}$$

where ε'_{zz} and ε''_{zz} denote its real and imaginary components: $\varepsilon_{zz} = \varepsilon'_{zz} + i\varepsilon''_{zz}$. It is evident that the imaginary part vanishes when $\omega < 2\mu/(1+|\beta_s|)$, and rises with the increase of the frequency of light when $2\mu/(1+|\beta_s|) < \omega < 2\mu/(1-|\beta_s|)$.

Lastly, the expression of off-diagonal term γ also displays complexity, but we want to obtain its analytical solution because of its important role in the excitation of the FR effect. Notably, when the tilt parameter meets $\beta < 1$, the expression of γ can be simply described as [41]

$$\gamma = \frac{\alpha}{\pi\omega}\left[2v_F Q - \sum_{s=\pm}\frac{s\mu}{2\beta_s}\left(\frac{1}{\beta_s}\ln\left|\frac{1+\beta_s}{1-\beta_s}\right| - 2\right)\right]. \tag{A5}$$

Obviously, γ exhibits a linear relationship with the frequency f of incident light and diminishes with the increase of frequency f for the fixed Q, μ, and β.

APPENDIX B: 4×4 MAGNETO-OPTICAL MOM

Firstly, the dispersion equation of wave vector in the WSM is studied by using Maxwell's equations. In regions 0, 1, and 2, the Maxwell's equations can be written as

$$\nabla \times \vec{E}_i = i\omega\mu_0\vec{H}_i, \tag{B1}$$

$$\nabla \times \vec{H}_i = -i\omega\vec{D}_i, \tag{B2}$$

where $i = 0,1,2$. Within the WSM, $i = 1$, by using the wave vector $\vec{k}_1$ to replace the spatial derivatives, Eqs. (B1) and (B2) can be expressed as $\vec{k}_1 \times \vec{E}_1 = \omega\mu_0\vec{H}_1$ and $\vec{k}_1 \times \vec{H}_1 = -\omega\varepsilon_0\overline{\overline{\varepsilon}}\vec{E}_1$, in which $\overline{\overline{\varepsilon}}$ denotes the tensor of the WSM. Simultaneously, we use $\vec{k}_1$ to cross the first equation above, and combine the second equation; thus the relationship between $\vec{k}_1$ and $\vec{E}_1$ can be expressed as

$$\vec{k}_1 \times (\vec{k}_1 \times \vec{E}_1) = -k_0^2\overline{\overline{\varepsilon}}\vec{E}_1. \tag{B3}$$

By using $\vec{k}_1 = k_{1x}\vec{x} + k_{1z}\vec{z}$, Eq. (B3) can be written as the matrix expression

$$\begin{pmatrix} k_0^2\varepsilon_{xx} - k_{1z}^2 & ik_0^2\gamma & k_{1z}k_{0x} \\ ik_0^2\gamma & k_\perp^2 - k_0^2\varepsilon_{xx} & 0 \\ k_{1z}k_{0x} & 0 & k_0^2\varepsilon_{zz} - k_{0x}^2 \end{pmatrix}\begin{pmatrix} E_{x1} \\ E_{y1} \\ E_{z1} \end{pmatrix} = 0, \tag{B4}$$

where $k_\perp = \sqrt{k_{1z}^2 + k_{1x}^2}$, $k_0 = \omega/c$, and $k_{0x} = k_0 \sin\theta$. Because of translational invariance, the transverse component of the wave vector is equal in each layer, $k_{1x} = k_{2x} = k_{0x}$. Due to the polarization separation of light propagating in the WSM, there exist three electric field components. The condition for the existence of a nonzero solution to the electric field in Eq. (B4) is that the modulus of the coefficient matrix is zero, so we can get the solution of k_{1z}, denoted by k_+ and k_- as

$$k_\pm^2 = \frac{k_0^2}{2\varepsilon_{zz}}\big[2\varepsilon_{xx}\varepsilon_{zz} - (\varepsilon_{xx} + \varepsilon_{zz})\sin^2\theta \pm \sqrt{(\varepsilon_{zz} - \varepsilon_{xx})^2\sin^4\theta - 4\varepsilon_{zz}\gamma^2\sin^2\theta + 4\varepsilon_{zz}^2\gamma^2}\big]. \tag{B5}$$

In order to obtain the calculation of the FR angle, the relevant transmission coefficients t_{pp} and t_{ps} should be calculated firstly, which are defined as $t_{pp} = E_t^p/E_i^p$ and $t_{ps} = E_t^s/E_i^p$, where E_i^p denotes the amplitude of the electric field of incident light for TM-polarized wave, and E_t^p and E_t^s exhibit the amplitude of the electric field of transmitted light for a TM- and transverse-electric (TE)-polarized wave.

For a TM-polarized wave, the incident magnetic field thus can be described as $\vec{H}_i = H_{y00}\vec{y}e^{i(k_{0x}x+k_{0z}z)}$. By using the Maxwell's equation $\nabla\times\vec{H} = -i\omega\vec{D}$, the corresponding incident electric field can be simply obtained as $\vec{E}_i = Z_0(\cos\theta\vec{x} - \sin\theta\vec{z})e^{i(k_{0x}x+k_{0z}z)}$, in which Z_0 denotes the wave impedance in vacuum, and the amplitude of the electric field is in units of H_{y00}. The incident light reflects at the contact surface of air and bulk WSM, resulting in the magnetic field in region 0 written in terms of incident and reflected waves, shown as

$$H_{x0} = r_3e^{-ik_{0z}z}e^{ik_{0x}x}, \quad H_{y0} = (e^{ik_{0z}z} + r_1e^{-ik_{0z}z})e^{ik_{0x}x}, \quad H_{z0} = r_2e^{-ik_{0z}z}e^{ik_{0x}x}. \tag{B6}$$

By using the Maxwell's equation $\nabla\cdot\vec{H}_0 = 0$, we get the relationship $r_3 = k_{0z}r_2/k_{0x}$. Meanwhile, by using $\nabla\times\vec{H} = -i\omega\vec{D}$, the electric field in region 0 is written as

$$E_{x0} = Z_0\frac{k_{0z}}{k_0}(e^{ik_{0z}z} - r_1e^{-ik_{0z}z})e^{ik_{0x}x}, \tag{B7}$$

$$E_{y0} = Z_0\frac{k_0}{k_{0x}}r_2e^{-ik_{0z}z}e^{ik_{0x}x}, \tag{B8}$$

$$E_{z0} = -Z_0\frac{k_{0x}}{k_0}(e^{ik_{0z}z} + r_1e^{-ik_{0z}z})e^{ik_{0x}x}. \tag{B9}$$

For region 1, the general solution of the electric field is described as a linear combination of the four wave-vector components $k_{1z} = \{k_+ \quad -k_+ \quad k_- \quad -k_-\}$:

$$E_{1y} = (a_1e^{ik_+z} + a_2e^{-ik_+z} + a_3e^{ik_-z} + a_4e^{-ik_-z})e^{ik_{0x}x}, \tag{B10}$$

by using Eqs. (B1) and (B2), the other components of the electric and magnetic fields can be obtained as

$$E_{1x} = \frac{i}{\gamma k_0^2}\big[\big(k_+^2 + k_{0x}^2 - \varepsilon_{//}k_0^2\big)(a_1e^{ik_+z} + a_2e^{-ik_+z}) + \big(k_-^2 + k_{0x}^2 - \varepsilon_{//}k_0^2\big)(a_3e^{ik_-z} + a_4e^{-ik_-z})\big]e^{ik_{0x}x}, \tag{B11}$$

$$E_{1z} = \frac{ik_{0x}}{\gamma k_0^2\big(k_{0x}^2 - \varepsilon_{zz}k_0^2\big)}\big[\big(k_+^2 + k_{0x}^2 - \varepsilon_{//}k_0^2\big)k_+(a_1e^{ik_+z} - a_2e^{-ik_+z}) + \big(k_-^2 + k_{0x}^2 - \varepsilon_{//}k_0^2\big)k_-(a_3e^{ik_-z} - a_4e^{-ik_-z})\big]e^{ik_{0x}x}, \tag{B12}$$

$$H_{1x} = -\frac{1}{Z_0k_0}(k_+a_1e^{ik_+z} - k_+a_2e^{-ik_+z} + k_-a_3e^{ik_-z} - k_-a_4e^{-ik_-z})e^{ik_{0x}x}, \tag{B13}$$

$$H_{1y} = \frac{-i\varepsilon_{zz}}{\gamma k_0Z_0\big(k_{0x}^2 - \varepsilon_{zz}k_0^2\big)}\big[\big(k_+^2 + k_{0x}^2 - \varepsilon_{//}k_0^2\big)k_+(a_1e^{ik_+z} - a_2e^{-ik_+z}) + \big(k_-^2 + k_{0x}^2 - \varepsilon_{//}k_0^2\big)k_-(a_3e^{ik_-z} - a_4e^{-ik_-z})\big]e^{ik_{0x}x}, \tag{B14}$$

$$H_{1z} = \frac{k_{0x}}{Z_0k_0}E_{1y}, \tag{B15}$$

where $\varepsilon_{//} = \varepsilon_{xx} = \varepsilon_{yy}$. For region 2, the transmitted light exists, and the corresponding magnetic field can be described as

$$H_{2x} = t_3e^{ik_{0z}(z-d)}e^{ik_{0x}x}, \quad H_{2y} = t_1e^{ik_{0z}(z-d)}e^{ik_{0x}x}, \quad H_{2z} = t_2e^{ik_{0z}(z-d)}e^{ik_{0x}x}. \tag{B16}$$

By using the Maxwell's equation $\nabla\cdot\vec{H}_2 = 0$, we get the relationship $t_3 = -k_{0z}t_2/k_{0x}$. Meanwhile, by using $\nabla\times\vec{H} = -i\omega\vec{D}$, the components of the electric field in region 2 are written as

$$E_{2x} = \frac{Z_0k_{0z}}{k_0}t_1e^{ik_{0z}(z-d)}e^{ik_{0x}x}, \tag{B17}$$

$$E_{2y} = \frac{Z_0k_0}{k_{0x}}t_2e^{ik_{0z}(z-d)}e^{ik_{0x}x}, \tag{B18}$$

$$E_{2z} = -\frac{Z_0k_{0x}}{k_0}t_1e^{ik_{0z}(z-d)}e^{ik_{0x}x}. \tag{B19}$$

Therefore, the components of the electric and magnetic fields in regions 0, 1, and 2 are all obtained. Notably, there exist eight parameters, $a_1, a_2, a_3, a_4, r_1, r_2, t_1$, and t_2, that need to be solved. Fortunately, upon matching the tangential electric and magnetic fields at $z = 0$ and $z = d$, we can calculate these parameters successfully. For calculating the parameters $(a_1 \quad a_2 \quad a_3 \quad a_4)$, a 4×4 matrix is established as

$$\begin{pmatrix} m_{11} & m_{12} & m_{13} & m_{14} \\ m_{21} & m_{22} & m_{23} & m_{24} \\ m_{31} & m_{32} & m_{33} & m_{34} \\ m_{41} & m_{42} & m_{43} & m_{44} \end{pmatrix} \begin{pmatrix} a_1 \\ a_2 \\ a_3 \\ a_4 \end{pmatrix} = \begin{pmatrix} 0 \\ -2i\gamma k_0 k_{0z} Z_0 \left(k_{0x}^2 - \varepsilon_{zz} k_0^2\right) \\ 0 \\ 0 \end{pmatrix}, \tag{B20}$$

where the parameters are as follows:

$$\begin{aligned}
&m_{11} = k_{0z} + k_+, \quad m_{12} = k_{0z} - k_+, \quad m_{13} = k_{0z} + k_-, \quad m_{14} = k_{0z} - k_- \\
&m_{31} = (k_+ - k_{0z})e^{ik_+d}, \quad m_{32} = (-k_+ - k_{0z})e^{-ik_+d}, \quad m_{33} = (k_- - k_{0z})e^{ik_-d}, \quad m_{34} = (-k_- - k_{0z})e^{-ik_-d}, \\
&m_{21} = -\varepsilon_{zz}k_{0z}k_+^3 + \left(k_{0x}^2 - \varepsilon_{zz}k_0^2\right)k_+^2 - \varepsilon_{zz}k_{0z}\left(k_{0x}^2 - \varepsilon_{//}k_0^2\right)k_+ + \left(k_{0x}^2 - \varepsilon_{zz}k_0^2\right)\left(k_{0x}^2 - \varepsilon_{//}k_0^2\right), \\
&m_{22} = \varepsilon_{zz}k_{0z}k_+^3 + \left(k_{0x}^2 - \varepsilon_{zz}k_0^2\right)k_+^2 + \varepsilon_{zz}k_{0z}\left(k_{0x}^2 - \varepsilon_{//}k_0^2\right)k_+ + \left(k_{0x}^2 - \varepsilon_{zz}k_0^2\right)\left(k_{0x}^2 - \varepsilon_{//}k_0^2\right), \\
&m_{23} = -\varepsilon_{zz}k_{0z}k_-^3 + \left(k_{0x}^2 - \varepsilon_{zz}k_0^2\right)k_-^2 - \varepsilon_{zz}k_{0z}\left(k_{0x}^2 - \varepsilon_{//}k_0^2\right)k_- + \left(k_{0x}^2 - \varepsilon_{zz}k_0^2\right)\left(k_{0x}^2 - \varepsilon_{//}k_0^2\right), \\
&m_{24} = \varepsilon_{zz}k_{0z}k_-^3 + \left(k_{0x}^2 - \varepsilon_{zz}k_0^2\right)k_-^2 + \varepsilon_{zz}k_{0z}\left(k_{0x}^2 - \varepsilon_{//}k_0^2\right)k_- + \left(k_{0x}^2 - \varepsilon_{zz}k_0^2\right)\left(k_{0x}^2 - \varepsilon_{//}k_0^2\right), \\
&m_{41} = \left[\varepsilon_{zz}k_{0z}k_+^3 + \left(k_{0x}^2 - \varepsilon_{zz}k_0^2\right)k_+^2 + \varepsilon_{zz}k_{0z}\left(k_{0x}^2 - \varepsilon_{//}k_0^2\right)k_+ + \left(k_{0x}^2 - \varepsilon_{zz}k_0^2\right)\left(k_{0x}^2 - \varepsilon_{//}k_0^2\right)\right]e^{ik_+d}, \\
&m_{42} = \left[-\varepsilon_{zz}k_{0z}k_+^3 + \left(k_{0x}^2 - \varepsilon_{zz}k_0^2\right)k_+^2 - \varepsilon_{zz}k_{0z}\left(k_{0x}^2 - \varepsilon_{//}k_0^2\right)k_+ + \left(k_{0x}^2 - \varepsilon_{zz}k_0^2\right)\left(k_{0x}^2 - \varepsilon_{//}k_0^2\right)\right]e^{-ik_+d}, \\
&m_{43} = \left[\varepsilon_{zz}k_{0z}k_-^3 + \left(k_{0x}^2 - \varepsilon_{zz}k_0^2\right)k_-^2 + \varepsilon_{zz}k_{0z}\left(k_{0x}^2 - \varepsilon_{//}k_0^2\right)k_- + \left(k_{0x}^2 - \varepsilon_{zz}k_0^2\right)\left(k_{0x}^2 - \varepsilon_{//}k_0^2\right)\right]e^{ik_-d}, \\
&m_{44} = \left[-\varepsilon_{zz}k_{0z}k_-^3 + \left(k_{0x}^2 - \varepsilon_{zz}k_0^2\right)k_-^2 - \varepsilon_{zz}k_{0z}\left(k_{0x}^2 - \varepsilon_{//}k_0^2\right)k_- + \left(k_{0x}^2 - \varepsilon_{zz}k_0^2\right)\left(k_{0x}^2 - \varepsilon_{//}k_0^2\right)\right]e^{-ik_-d}
\end{aligned}$$

.

After obtaining the calculation of the four parameters $(a_1 \quad a_2 \quad a_3 \quad a_4)$, the other four parameters can be obtained as

$$r_1 = 1 - \frac{i}{\gamma k_0 k_{0z} Z_0}\left(k_+^2 + k_{0x}^2 - \varepsilon_{//}k_0^2 \quad k_+^2 + k_{0x}^2 - \varepsilon_{//}k_0^2 \quad k_-^2 + k_{0x}^2 - \varepsilon_{//}k_0^2 \quad k_-^2 + k_{0x}^2 - \varepsilon_{//}k_0^2\right)\begin{pmatrix} a_1 \\ a_2 \\ a_3 \\ a_4 \end{pmatrix}, \tag{B21}$$

$$r_2 = \frac{k_{0x}}{k_0 Z_0}(1 \quad 1 \quad 1 \quad 1)\begin{pmatrix} a_1 \\ a_2 \\ a_3 \\ a_4 \end{pmatrix}, \tag{B22}$$

$$t_2 = -\frac{k_{0x}}{k_{0z} k_0 Z_0}\left(-k_+e^{ik_+d} \quad k_+e^{-ik_+d} \quad -k_-e^{ik_-d} \quad k_-e^{-ik_-d}\right)\begin{pmatrix} a_1 \\ a_2 \\ a_3 \\ a_4 \end{pmatrix}, \tag{B23}$$

$$t_1 = \frac{-i\varepsilon_{zz}}{\gamma k_0 Z_0\left(k_{0x}^2 - \varepsilon_{zz}k_0^2\right)} C \begin{pmatrix} a_1 \\ a_2 \\ a_3 \\ a_4 \end{pmatrix}, \tag{B24}$$

$$C = \left[\left(k_+^2 + k_{0x}^2 - \varepsilon_{//}k_0^2\right)k_+e^{ik_+d} \quad -\left(k_+^2 + k_{0x}^2 - \varepsilon_{//}k_0^2\right)k_+e^{-ik_+d} \quad \left(k_-^2 + k_{0x}^2 - \varepsilon_{//}k_0^2\right)k_-e^{ik_-d} \quad -\left(k_-^2 + k_{0x}^2 - \varepsilon_{//}k_0^2\right)k_-e^{-ik_-d}\right]. \tag{B25}$$

Finally, we can get the transmission coefficients, t_{pp} and t_{ps}, written as

$$t_{pp} = \frac{E_t^p}{E_i^p} = t_1, \tag{B26}$$

$$t_{ps} = \frac{E_t^s}{E_i^p} = \frac{k_0}{k_{0x}} t_2. \tag{B27}$$

[1] M. Mansuripur, *The Physical Principles of Magneto-Optical Recording* (Cambridge University Press, Cambridge, 1998).
[2] M. Freiser, IEEE Trans. Magn. **4**, 152 (1968).
[3] J.-W. Tioh, M. Mina, and R. J. Weber, IEEE Trans. Magn. **46**, 2474 (2010).
[4] M. Tamagnone, C. Moldovan, J.-M. Poumirol, A. B. Kuzmenko, A. M. Ionescu, J. R. Mosig, and J. Perruisseau-Carrier, Nat. Commun. **7**, 11216 (2016).
[5] K. B. Rochford, A. H. Rose, M. N. Deeter, and G. W. Day, Opt. Lett. **19**, 1903 (1994).
[6] H. Kato, T. Matsushita, A. Takayama, M. Egawa, K. Nishimura, and M. Inoue, J. Appl. Phys. **93**, 3906 (2003).
[7] M. Liu and X. Zhang, Nat. Photon. **7**, 429 (2013).
[8] I. S. Maksymov, Nanomaterials **5**, 577 (2015).
[9] Y. Liang, Y. Xiang, and X. Dai, Opt. Express **28**, 24560 (2020).
[10] D. Dong, Y. Liu, and Y. Fu, Appl. Opt. **59**, 9607 (2020).
[11] A. Christofi, Y. Kawaguchi, and A. Khanikaev, Opt. Lett. **43**, 1838 (2018).
[12] A. A. Burkov and L. Balents, Phys. Rev. Lett. **107**, 127205 (2011).
[13] C. K. Chan, P. A. Lee, K. S. Burch, J. H. Han, and Y. Ran, Phys. Rev. Lett. **116**, 026805 (2016).
[14] N. P. Armitage, E. J. Mele, and A. Vishwanath, Rev. Mod. Phys. **90**, 015001 (2018).
[15] E. Hendry, P. J. Hale, J. Moger, A. K. Savchenko, and S. A. Mikhailov, Phys. Rev. Lett. **105**, 097401 (2010).
[16] S. Shareef, Y. S. Ang, and C. Zhang, J. Opt. Soc. Am. B **29**, 274 (2012).
[17] L. Ju, B. Geng, J. Horng, C. Girit, M. Martin, Z. Hao, H. A. Bechtel, X. Liang, A. Zettl, Y. R. Shen, and F. Wang, Nat. Nanotechnol. **6**, 630 (2011).
[18] A. A. Zyuzin and A. A. Burkov, Phys. Rev. B **86**, 115133 (2012).
[19] E. Liu, Y. Sun, N. Kumar, L. Meuchler, A. Sun, J. Lin, S. Yang, D. Liu, A. Liang, Q. Xu, J. Kroder, V. Seuss, H. Borrmann, C. Shekhar, Z. Wang, C. Xi, W. Wang, W. Schnelle, S. Wirth, Y. Chen *et al.*, Nat. Phys. **14**, 1125 (2018).
[20] Y. Ferreiros, A. A. Zyuzin, and J. H. Bardarson, Phys. Rev. B **96**, 115202 (2017).
[21] P. Hosur, S. A. Parameswaran, and A. Vishwanath, Phys. Rev. Lett. **108**, 046602 (2012).
[22] S. Wang, B. Lin, A. Wang, D. Yu, and Z. Liao, Adv. Phys.: X **2**, 518 (2017).
[23] K. Das and A. Agarwal, Phys. Rev. B **99**, 085405 (2019).
[24] F. Wilczek, Phys. Rev. Lett. **58**, 1799 (1987).
[25] L. Wu, M. Salehi, N. Koirala, J. Moon, S. Oh, and N. P. Armitage, Science **354**, 1124 (2016).
[26] O. V. Kotov and Y. E. Lozovik, Phys. Rev. B **93**, 235417 (2016).
[27] M. Kargarian, M. Randeria, and N. Trivedi, Sci. Rep. **5**, 12683 (2015).
[28] J. Wu, R. Zeng, J. Liang, L. Jiang, and Y. Jiang, J. Appl. Phys. **129**, 153103 (2021).
[29] K. Sonowal, A. Singh, and A. Agarwal, Phys. Rev. B **100**, 085436 (2019).
[30] G. Ye, W. Zhang, W. Wu, S. Chen, W. Shu, H. Luo, and S. Wen, Phys. Rev. A **99**, 023807 (2019).
[31] G. Jia, Z. Huang, Q. Ma, and G. Li, Nanophotonics **9**, 715 (2020).
[32] H. Dai, Q. Song, H. Ye, and X. Yan, Appl. Phys. Lett. **119**, 081103 (2021).
[33] J. Wu, L. Jiang, R. Zeng, J. Liang, X. Dai, and Y. Xiang, Phys. Rev. A **105**, 023508 (2022).
[34] R. W. Ziolkowski, Phys. Rev. E **70**, 046608 (2004).
[35] I. Liberal and N. Engheta, Nat. Photon. **11**, 149 (2017).
[36] X. Niu, X. Hu, S. Chu, and Q. Gong, Adv. Opt. Mater. **6**, 1701292 (2018).
[37] Y. Sha, J. Wu, Z. T. Xie, H. Y. Fu, and Q. Li, IEEE Photon. J. **13**, 4800412 (2021).
[38] P. P. Edwards, A. Porch, M. O. Jones, D. V. Morgan, and R. M. Perks, Dalton Trans. **19**, 2995 (2004).
[39] X. Liu, K. Zhang, J. H. Kang, J. Park, J. S. Harris, P. G. Kik, and M. L. Brongersma, ACS Photon. **5**, 4484 (2018).
[40] F. Michelotti, L. Dominici, E. Descrovi, N. Danz, and F. Menchini, Opt. Lett. **34**, 839 (2009).
[41] K. Halterman, M. Alidoust, and A. Zyuzin, Phys. Rev. B **98**, 085109 (2018).
[42] K. Halterman and M. Alidoust, Opt. Express **27**, 36164 (2019).
[43] A. G. Grushin, J. W. F. Venderbos, and J. H. Bardarson, Phys. Rev. B **91**, 121109(R) (2015).
[44] P. Rodriguez-Lopez, A. Popescu, I. Fialkovsky, N. Khusnutdinov, and L. M. Woods, Commun. Mater. **1**, 14 (2020).
[45] M. Born and E. Wolf, *Principles of Optics*, 7th ed. (Cambridge University Press, Cambridge, 1999).
[46] S. Visnovsky, *Optics in Magnetic Multilayers and Nanostructures, Optical Science and Engineering* (CRC Press, Boca Raton, FL, 2006).
[47] G. Széchenyi, M. Vigh, A. Kormányos, and C. József, J. Phys.: Condens. Matter **28**, 375802 (2016).
[48] B. Xu, Y. M. Dai, L. X. Zhao, K. Wang, R. Yang, W. Zhang, J. Y. Liu, H. Xiao, G. F. Chen, A. J. Taylor, D. A. Yarotski, R. P. Prasankumar, and X. G. Qiu, Phys. Rev. B **93**, 121110(R) (2016).
[49] M. Chinotti, A. Pal, W. J. Ren, C. Petrovic, and L. Degiorgi, Phys. Rev. B **94**, 245101 (2016).
[50] E. Haubold, K. Koepernik, D. Efremov, S. Khim, A. Fedorov, Y. Kushnirenko, J. van den Brink, S. Wurmehl, B. Buchner, T. K. Kim, M. Hoesch, K. Sumida, K. Taguchi, T. Yoshikawa, A. Kimura, T. Okuda, and S. V. Borisenko, Phys. Rev. B **95**, 241108(R) (2017).